



Polarization modulation by surface plasmons in Young's double-slit setup

Aleksi Leinonen ^{1,*}, Kimmo Saastamoinen,¹ Henri Pesonen,¹ Gaofeng Wu,² Taco D. Visser ^{3,4},
Jari Turunen,¹ and Ari T. Friberg¹

¹*Institute of Photonics, University of Eastern Finland, P.O. Box 111, 80101 Joensuu, Finland*

²*School of Physics, Northwest University, Xi'an 710069, China*

³*Department of Physics and Astronomy, Vrije Universiteit, Amsterdam 1081 HV, Netherlands*

⁴*Institute of Optics, University of Rochester, Rochester, New York 14627, USA*



(Received 18 May 2021; accepted 20 September 2021; published 6 October 2021)

A simple phenomenological model, justified by rigorous electromagnetic analysis, is used to examine far-field polarization modulation introduced by a metallic screen with two subwavelength slits in uniform, partially polarized illumination. The accuracy of this intuitive model is assessed numerically, by employing the Fourier modal method, as regards the wavelength, the screen metal, and the slit depth, width, and separation. The Stokes parameters and the degree of polarization are evaluated paraxially in the far zone of the slits. We demonstrate that a uniform, partially linearly polarized incident beam can be rendered unpolarized by the nanoslits. Our work provides insight into the pivotal role that surface plasmons have in polarization modulation in photonics.

DOI: [10.1103/PhysRevA.104.043503](https://doi.org/10.1103/PhysRevA.104.043503)

I. INTRODUCTION

Extraordinary optical transmission (EOT) [1], variably attributed to the effects of surface plasmon polaritons (SPPs), waveguide modes, optical vortices, and Fabry-Pérot-type resonances in subwavelength metallic structures [2–5], has aroused much interest in plasmonics since its initial observation. There has been a surge in plasmonic nanophotonics research, which has led to a number of potential applications [6–10]. To date, the SPPs have been observed to control the transmission [11] and spatial coherence [10,12,13] of incident light, demonstrated by Young's classic two-beam setup with subwavelength slits fabricated in a thin metallic layer. In this work we consider the modulation of the polarization state of light caused by surface plasmon effects by making use of a simple phenomenological model. The value of this model lies in the fact that it is computationally fast and efficient, exhaustive in terms of materials and wavelengths, and amenable to future extensions. In particular, the model describes conceptually and reasonably accurately the physical mechanism that underlies optical diffraction by nanoapertures, namely, the interplay between direct transmission and SPPs generated at adjacent apertures. The model has previously been successfully applied to explain both EOT [11] and coherence modulation [12,13] by showing that in Young's double-slit experiment the field properties vary harmonically with slit separation, with a period determined by the SPP wavelength. We further explicitly confirm the accuracy of this intuitive model by rigorous numerical simulations.

We begin by presenting, in Sec. II, an electromagnetic extension of a widely employed phenomenological model [11,12] for a plasmon-assisted Young double-slit experiment,

restricting attention to uniform, partially polarized plane-wave illumination. The application of this model requires the determination of certain transmission and scattering factors. The evaluation of these coefficients by means of rigorous diffraction theory, the Fourier modal method [14], is the subject of Sec. III. The range of validity of the model is investigated in Sec. IV under various conditions and for different materials and wavelengths. We demonstrate that the model is highly accurate provided the slit separation is sufficiently large to ignore multiple reflections of the plasmons between the slits. In Sec. V we present analytical and numerical results on the polarization-state modulation, in terms of the Stokes parameters and the degree of polarization, which occur in a plasmon-assisted Young experiment. We show in particular that an incident partially linearly polarized beam field may be rendered strictly unpolarized by the setup. The main conclusions of this work are summarized in Sec. VI. Certain mathematical developments are relegated to Appendixes A and B.

II. PHENOMENOLOGICAL MODEL

The optical configuration that we study is illustrated schematically in Figs. 1 and 2. A plane electromagnetic wave of free-space wavelength λ_0 is normally incident on a metallic screen confined between planes $z = 0$ and $z = d$. Two subwavelength slits (of width $w < \lambda_0$) are pierced into the screen, with center-to-center spacing a . Light is transmitted by these slits into the half space $z > d$, taken to be vacuum ($n = 1$), and subsequently propagates into the far zone, forming a Young interference pattern there. Our interest is finding the state of polarization of the light in the far-zone paraxial region and comparing that with the polarization of the incident plane wave.

*Corresponding author: aleksi.leinonen@uef.fi

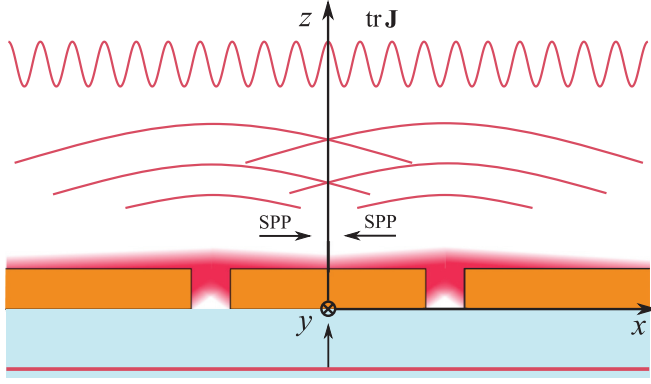


FIG. 1. Illustration of the physical situation. Propagating fields and the final interference pattern are shown with red solid lines; evanescent fields are displayed with red shading. The far-zone interference pattern $\text{tr } \mathbf{J}$ at height z is created by the two beams emerging from the slits. Surface plasmon waves, which affect the far-field interference pattern, are presented as arrows.

In the phenomenological model we treat the slits as secondary line sources, which radiate cylindrical waves. In s polarization (or TE, with the electric vector in the y direction) the response of a single slit to unit-amplitude illumination is described by a complex transmission factor β . In p polarization (or TM, with the electric vector in the x direction) the complex transmission factor under unit-amplitude illumination is denoted by α . However, in this case the field transmitted through one slit also excites a surface plasmon that propagates towards the other slit and is scattered into a freely propagating field in the half space $z > d$, with an excitation and scattering factor γ . Hence, the field emanating from one slit is given by $\alpha + \gamma K$, where $K = \exp(ik_{\text{sp}}a)$ is a modulation factor due to SPP propagation between the slits separated by distance a . Further, $k_{\text{sp}} = k_0 n / \sqrt{1 + n^2}$ [15] is the complex plasmon propagation constant, k_0 is the vacuum wave number, and n is the (complex) refractive index of the metal.

Considering a general, partially polarized plane-wave illumination, we define the polarization state of the incident field

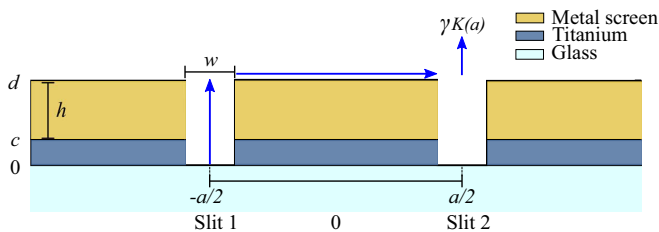


FIG. 2. Geometry of the double-slit system used in rigorous calculations, when both slits are open. The blue arrows illustrate how the SPPs generated in slit 1 travel to slit 2 and subsequently scatter into the far zone. The thickness of the metal screen is h , i.e., $d = h + c$, where c is the Ti film depth. The role of the thin Ti layer is merely to prevent plasmon propagation on the lower metal surface.

at $z = 0$ by a polarization matrix

$$\mathbf{J}^i = \begin{bmatrix} J_{pp} & J_{ps} \\ J_{sp} & J_{ss} \end{bmatrix}, \quad (1)$$

normalized such that $\text{tr } \mathbf{J}^i = 1$. With the notation for transmission factors of the slits defined above, the polarization matrix in the paraxial region of the far zone takes the form (see Appendix A for more details)

$$\mathbf{J}(\theta) = \cos^2\left(\frac{ak_0\theta}{2}\right) \Phi, \quad (2)$$

where θ is the diffraction angle and

$$\begin{aligned} \Phi &= \begin{bmatrix} \Phi_{xx} & \Phi_{xy} \\ \Phi_{yx} & \Phi_{yy} \end{bmatrix} \\ &= \begin{bmatrix} J_{pp}|\alpha + \gamma K|^2 & J_{ps}\beta(\alpha + \gamma K)^* \\ J_{sp}\beta^*(\alpha + \gamma K) & J_{ss}|\beta|^2 \end{bmatrix}. \end{aligned} \quad (3)$$

Hence we observe a cosinusoidal interference pattern of unit visibility, multiplied by a constant matrix Φ defining the far-field polarization state. Consequently, we can calculate the Stokes parameters [16]

$$S_0 = \Phi_{xx} + \Phi_{yy}, \quad (4)$$

$$S_1 = \Phi_{xx} - \Phi_{yy}, \quad (5)$$

$$S_2 = \Phi_{xy} + \Phi_{yx}, \quad (6)$$

$$S_3 = i[\Phi_{yx} - \Phi_{xy}] \quad (7)$$

and their normalized forms $s_j = S_j/S_0$, $j \in \{1, 2, 3\}$, as well as the degree of polarization

$$P = \frac{\sqrt{S_1^2 + S_2^2 + S_3^2}}{S_0} \quad (8)$$

in the paraxial far zone of the double-slit structure.

III. DETERMINATION OF TRANSMISSION AND SCATTERING FACTORS

Use of the phenomenological model to study the polarization modulation effects requires that we know the set of the slit's transmission and scattering factors (α, β, γ) . We make use of the Fourier modal method (FMM) [14] to estimate these parameters, although several other rigorous diffraction analysis methods could be employed equally well. An advantage of the model over these rigorous methods is that once the coefficients have been determined, they can be used to explore various physical effects without the need for further computationally extensive rigorous calculations. As an example we may cite slit separation: A change in it leads to adjustments in the computational window with cubic computing-time dependence (FMM) on the window width, whereas a similar change when employing the model has no influence. We consider the physical arrangement illustrated in Fig. 2, where the metal screen is fabricated on a substrate. The purpose of the titanium layer between the metal and the substrate is to suppress plasmon propagation on the input surface $z = 0$.

The factor β is evaluated by considering a purely s -polarized unit-amplitude illumination and calculating the E_y component of the field at the plane $z = d$ for a single slit

at its center point. The factor α is determined similarly by computing the E_x component on p -polarized unit-amplitude illumination.

To determine γ we leave slit 1 open, but block direct transmission through slit 2, and then evaluate $J_{xx}(\theta)$. In the FMM analysis, blocking is effected by adding a slab of Ti in front of the slit at the plane $z = 0$ (see Fig. 2). Since slit 2 then produces only a scattered contribution due to the plasmon propagation from slit 1, we obtain an interference pattern of reduced visibility and an offset of the central maximum from the direction $\theta = 0$. In terms of the phenomenological model, we now have

$$J_{xx}(\theta) = |\alpha|^2 + |\gamma|^2 \exp[-2 \operatorname{Im}(k_{\text{sp}})a] + 2|\alpha||\gamma| \exp[-\operatorname{Im}(k_{\text{sp}})a] \times \cos[\arg \gamma - \arg \alpha + \operatorname{Re}(k_{\text{sp}})a - k_0 \theta a], \quad (9)$$

where Re and Im denote the real and imaginary parts, respectively. The phase of γ is obtained from the offset of the cosine term, i.e.,

$$\arg \gamma = \arg \alpha + [k_0 \theta_0 - \operatorname{Re}(k_{\text{sp}})]a, \quad (10)$$

where θ_0 is the angular position of the shifted central maximum. The absolute value of γ is determined from the visibility $V = (J_{\max} - J_{\min})/(J_{\max} + J_{\min})$ of the interference pattern,

$$|\gamma| = |\alpha| \left(\frac{1}{V} - \sqrt{\frac{1}{V^2} - 1} \right) \exp[\operatorname{Im}(k_{\text{sp}})a]. \quad (11)$$

The complex γ is determined by the offset and the visibility of the interference pattern calculated by the FMM (normalized by the single-slit radiation pattern) using a sufficiently large value of slit separation a to effectively suppress the effects of multiple scattering of the surface plasmons between the slits. In practice, we choose a to be of the order of the SPP survival (decay) length.

As an example of estimating the coefficients α , β , and γ we consider a gold-air interface at vacuum wavelength $\lambda_0 = 740$ nm. The SPP decay length in this case is $l_{\text{sp}} = 1/\operatorname{Im}(k_{\text{sp}}) \approx 114.5$ μm , which we use as the slit separation a . The slit width and depth are $w = 250$ nm and depth $h = 200$ nm, respectively, and the Ti layer thickness $c = 20$ nm. In the one-slit case, a Ti cover of thickness 1 μm and width $a/2$ is placed on the input of slit 2. The resulting transmission coefficients are $\alpha = 0.377 + 0.211i$ and $\beta = -0.115 - 0.258i$.

Whereas in the two-slit case the coefficients γ and K are separated in the phenomenological model, a small quasiperiodic variation in γ remains in the rigorous FMM simulations, as is illustrated for the absolute value in Fig. 3(a). The period of this fluctuation is equal to $\lambda_{\text{sp}} = 2\pi/\operatorname{Re}(k_{\text{sp}}) = 720$ nm, suggesting that the variation originates from the SPP's actual phase which at the exit slit depends on the separation a . To obtain a constant value for the coefficient γ , we therefore take an average over the fluctuation period by varying a within the range 114.5 – 115.9 μm , which in this case gives $\gamma = -0.050 - 0.101i$.

Although the quasiperiodic variation of γ is averaged out, the Stokes parameters still are left with small quasiperiodic oscillations because of the term K in Eq. (3); these are shown

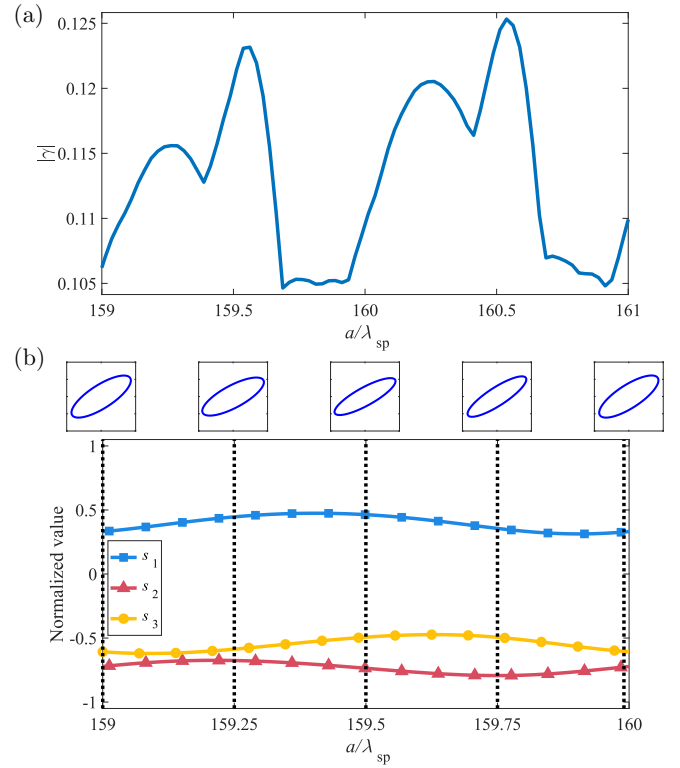


FIG. 3. Fluctuation of (a) $|\gamma|$ for $159\lambda_{\text{sp}} \leq a \leq 161\lambda_{\text{sp}}$ and (b) oscillation of the normalized far-field Stokes parameters s_1 (blue squares), s_2 (red triangles), and s_3 (yellow circles) for $159\lambda_{\text{sp}} \leq a \leq 160\lambda_{\text{sp}}$, with the corresponding polarization states presented as ellipses, for a uniform 45° linearly polarized input field.

in Fig. 3(b). Paraxially, the diffracted field, resulting from a 45° linearly polarized uniform illumination, is no longer linearly polarized (s_3 differs from zero), but rather elliptically polarized, as is explicitly illustrated in the figure. We observe that the emerging elliptically polarized electric fields contain considerable x and y components, since $|\alpha|$ and $|\beta|$ are roughly of equal size.

The coefficients α , β , and γ naturally depend on the metal and the wavelength, as well as on the values of the slit width and depth. Figure 4 shows a more systematic study of the coefficient dependence on the width w and depth h of the slits for the structure considered above (Au and air, $\lambda_0 = 740$ nm, Fig. 2). The solid lines illustrate the variations when the slit depth is fixed at $h = 200$ nm and the width is scanned. The dashed lines show the results when the width is fixed at $w = 250$ nm and the slit depth is varied. We restrict the scanning range of w to below $\lambda_0/2$ to retain the subwavelength nature of the slit. On the other hand, we limit the range of h to values above 150 nm to prevent light from penetrating through the solid part of the metal screen. The values of γ are evaluated around slit separation $a = 97.75\lambda_{\text{sp}}$.

Considering the transmission coefficients, $|\alpha|$ depends only weakly on h and grows nearly linearly with w . On the other hand, $|\beta|$ is reduced when h increases but increases with w . These results are expected in view of the theory of metal-insulator-metal waveguides. The ratio of the scattering coefficient $|\gamma|$ to $|\alpha|$ is nearly independent of h , but depends

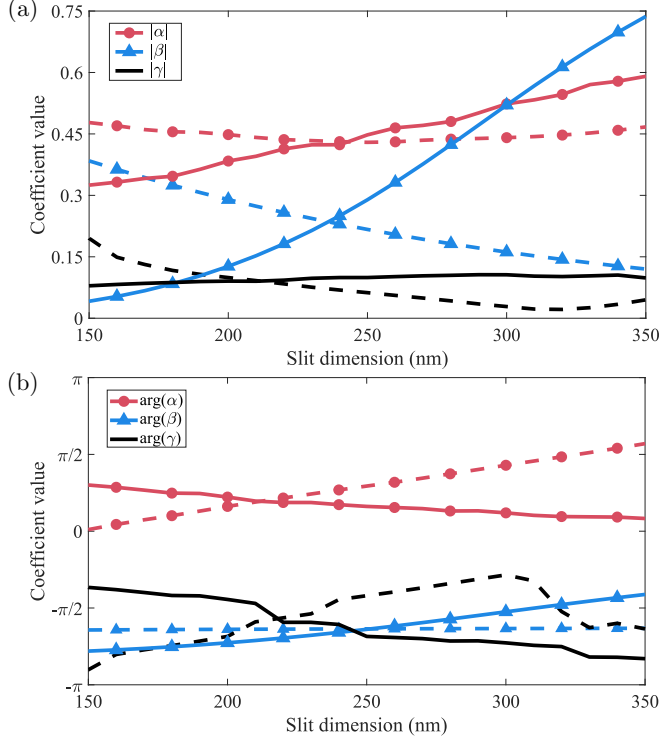


FIG. 4. Numerically estimated values of (a) $|\alpha|$, $|\beta|$, and $|\gamma|$ and (b) phases of α , β , and γ for a gold-air double slit at $\lambda_0 = 740$ nm and $a = 97.75\lambda_{sp}$. The solid lines correspond to $h = 200$ nm and w is varied. The dashed lines represent the case when $w = 250$ nm and h is varied. Red (circles) corresponds to α , blue (triangles) to β , and black to γ .

on w . The values $w = 250$ nm and $h = 200$ nm represent a good compromise and will therefore be used in our analyses from now on.

IV. VALIDITY OF THE MODEL

The phenomenological model takes into account only one-directional plasmon propagation from one slit to the other. It thus ignores the phenomena of back (and multiple) reflections of the SPPs, which grow stronger when the slit separation is small in relation to the plasmon survival distance, i.e., $a \ll l_{sp}$. All such effects are nonetheless fully accounted for in the FMM analysis. We note that the simple model could be enhanced by incorporating backpropagation phenomena as well [17].

We consider three metals and several wavelengths in the model validity analysis: gold (620 and 740 nm), silver (600, 700, and 800 nm), and aluminium (460, 560, and 660 nm). The geometry of Fig. 2 is used, with the same structure parameters for all cases. The values of slit separation a are taken at the maximum intensity points $a = (n + \frac{1}{2})\lambda_{sp}$ [11], starting from $n = 5$, with an interval of λ_{sp} up to $a = 3l_{sp}/4$, after which we use an interval of $4\lambda_{sp}$. The interval is increased here since comparable results are obtained with the model and the FMM, but the latter experiences a drastic increase in computing time and memory usage. We calculate α , β , and γ in the same fashion as before, and normalize the phenomeno-

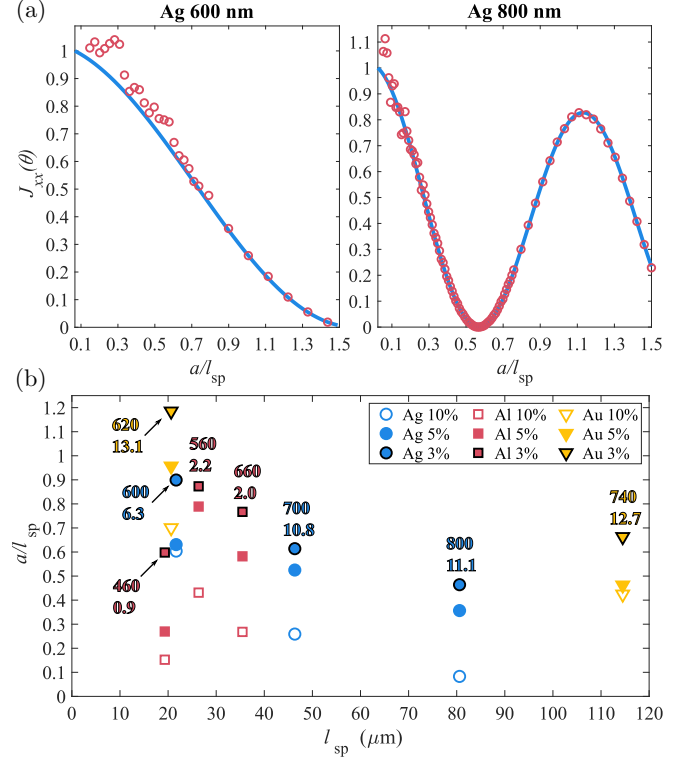


FIG. 5. Deviations between the phenomenological model and the FMM simulations. (a) Plots of $J_{xx}(\theta)$ as a function of the slit separation for silver at wavelengths 600 nm and 800 nm. The blue solid line is the phenomenological model of Eq. (12) and red circles are the results of FMM calculations. (b) Maximum relative error after a certain a/l_{sp} as a function of the SPP decay length for all cases. Marked next to the calculated points are the wavelength in nanometers (top) and $|\gamma|^2 \times 10^{-3}$ (bottom).

logical model such that it coincides with the FMM results at slit separation closest to point $a = 1.2l_{sp}$, and scale the value of the model to unity at the starting point for the phenomenological model ($a = 7\lambda_{sp}/2$). The normalization point should be far enough to remove the effects of plasmon backscattering completely. The far-field interference pattern for the phenomenological model with two slits open is derived in the same fashion as Eq. (9) (see Appendix A),

$$J_{xx}(\theta) = \{|\alpha|^2 + |\gamma|^2 \exp[-2\text{Im}(k_{sp})a] + 2|\alpha||\gamma| \exp[-\text{Im}(k_{sp})a] \times \cos[\arg \gamma - \arg \alpha + \text{Re}(k_{sp})a]\} \times \cos^2\left(\frac{ak_0\theta}{2}\right), \quad (12)$$

for fully p -polarized incident light. We consider the angle $\theta = 0.5^\circ$ in all the cases of comparison between the phenomenological and FMM results to acquire a better understanding of the accuracy of the model when the slit separation is varied. The interference pattern in Eq. (12) reaches zero when the last cosine term vanishes, i.e., when $ak_0\theta/2 = \pi$, from which we explicitly find the zero point at $a/l_{sp} = 0.5\text{Im}(k_{sp})\lambda_0/\theta$.

Figure 5(a) shows $J_{xx}(\theta)$ as well as the numerically obtained p -polarized far-field intensity for silver at 600 and

800 nm. The cosine term in Eq. (12) becomes zero when $a/l_{\text{sp}} \approx 1.59$ and 0.57 , respectively. The phenomenological model and the FMM results are observed to deviate somewhat when $a \ll l_{\text{sp}}$, as can be expected due to multiple traversals of the SPPs between the slits. However, the agreement is excellent for larger values of a where only single-scattered plasmons contribute to the far-field interference pattern.

Figure 5(b) shows the relative deviations between the FMM results and the phenomenological model as a function of l_{sp} for all the metals and wavelengths considered. The vertical axis represents the value of a/l_{sp} where the difference has (roughly) decreased below 10%, 5%, and 3%. The numbers accompanying each data point indicate the wavelength (in nanometers, top) and the value of $|\gamma|^2 \times 10^{-3}$ (bottom). The minimum separations a , where the model's accuracy reaches a desired level, vary with both wavelength and metal. Obviously the SPP strength also plays a role, which can partly be seen from the values of $|\gamma|^2$ and partly from the long decay lengths. Another significant factor here is the ratio of the incident light's wavelength to the slit width, λ_0/w . The phenomenological model is valid only when $w \ll \lambda_0$, which is not always fully the case in Fig. 5(b), for instance, aluminium at 460 nm ($\lambda_0/w = 1.84$).

V. POLARIZATION MODULATION

In this section we make use of the phenomenological model to analyze polarization-state modulation by the metallic double-slit structure. We consider uniform, partially linearly polarized illumination and represent the associated polarization matrix \mathbf{J}^i as a sum of the unpolarized and fully polarized parts. We may then express its elements as (see Appendix B)

$$J_{\text{pp}} = \frac{1}{2}(1 - P^i) + P^i \cos^2 \phi, \quad (13)$$

$$J_{\text{ps}} = J_{\text{sp}} = P^i \sin \phi \cos \phi, \quad (14)$$

$$J_{\text{ss}} = \frac{1}{2}(1 - P^i) + P^i \sin^2 \phi, \quad (15)$$

where P^i is the degree of polarization of the input field and ϕ is the polarization angle of the linearly polarized part measured from the x direction. Inserting these expressions into Eq. (3), we can determine the elements of the matrix Φ and consequently the Stokes parameters given by Eqs. (4)–(7) (see Appendix B for the explicit expressions) along with the far-field degree of polarization P as functions of P^i and ϕ .

Figure 6 illustrates the behavior of the normalized Stokes parameters s_j , $j \in \{1, 2, 3\}$, and the degree of polarization P in the far zone as a function of P^i for selected values of ϕ . In the numerical examples we consider gold and take $w = 250$ nm and $h = 200$ nm. With these values we find $\alpha = 0.377 + 0.211i$, $\beta = -0.115 - 0.258i$, and $\gamma = -0.050 - 0.101i$, as before, and $K = 8.7261 + 0.0087i$, which corresponds to a slit separation $a = 115$ μm and Au at wavelength $\lambda_0 = 740$ nm. The dashed lines indicate the cases when plasmon-assisted effects are ignored, i.e., we have set $\gamma = 0$. Hence the difference between the solid and dashed lines indicates the influence of the SPPs, which is clearly observable even for the relatively large value of a considered here, and grows substantially for smaller slit separations.

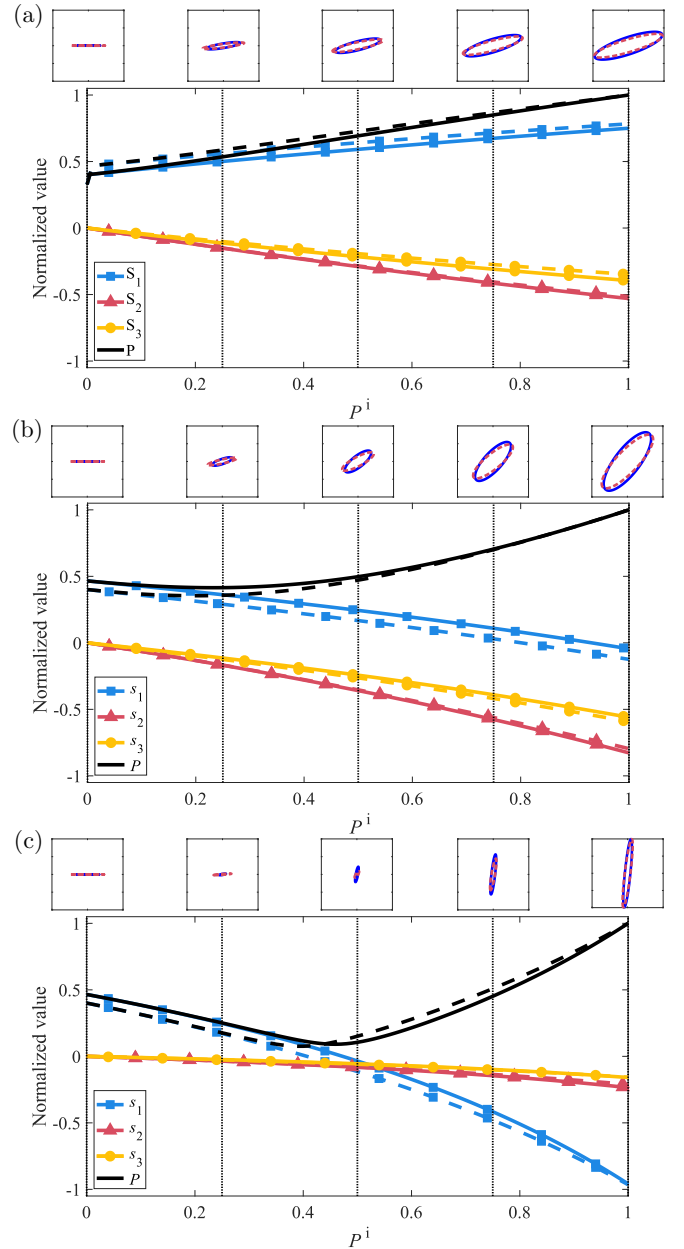


FIG. 6. Polarization properties in the far field as a function of the input degree of polarization P^i for (a) $\phi = 30^\circ$, (b) $\phi = 60^\circ$, and (c) $\phi = 85^\circ$ linearly polarized light. The dashed lines correspond to the case $\gamma = 0$. The blue (squares) lines present s_1 , red (triangles) s_2 , and yellow (circles) s_3 . In the polarization ellipses the red dashed line corresponds to maxima and the blue solid line to minima in Fig. 3.

For small values of ϕ , P increases monotonically with P^i . However, in a certain range of ϕ and P^i we observe a minimum for P . A closer study shows that for P to attain a minimum, the condition $S_1 = 0$ must be satisfied. Using Eqs. (B5)–(B8), we readily find that this requires

$$P^i = -\frac{|\alpha + \gamma K|^2 - |\beta|^2}{(|\alpha + \gamma K|^2 + |\beta|^2) \cos(2\phi)}, \quad (16)$$

assuming that $|\alpha + \gamma K| \geq |\beta|$ admissible solutions with $0 \leq P^i \leq 1$ are found in the range $\phi_c \leq \phi \leq \pi - \phi_c$, where

$$\phi_c = \frac{1}{2} \arccos \left(\frac{|\beta|^2 - |\alpha + \gamma K|^2}{|\alpha + \gamma K|^2 + |\beta|^2} \right). \quad (17)$$

However, the condition that $S_1 = 0$ is not sufficient for the light paraxially in the far zone to be unpolarized, but additionally it is necessary that the off-diagonal elements of the polarization matrix Φ in Eq. (3) are zero. If $S_1 = 0$, the degree of polarization in the far zone takes the form $P = |\Phi_{xy}|/S_0$. From Eqs. (B6) and (B9) we then find

$$P = \frac{(|\alpha + \gamma K|^2 - |\beta|^2) \sin(2\phi)}{4|\alpha + \gamma K||\beta| \cos(2\phi)}, \quad (18)$$

which shows that unpolarized output in the paraxial direction in these circumstances is possible only if $\phi = \pi/2$ or $|\alpha + \gamma K|^2 = |\beta|^2$. If, on the other hand, $|\beta| \geq |\alpha + \gamma K|$, then solutions with $0 \leq P^i \leq 1$ yielding $S_1 = 0$ are found in the range $-\phi_c \leq \phi \leq \phi_c$. Besides $|\alpha + \gamma K|^2 = |\beta|^2$ as above, in this case a paraxially unpolarized output field is possible only if $\phi = 0$. It should be noted, though, that $|\beta| \geq |\alpha + \gamma K|$ would normally not occur with subwavelength metal slits, which are the basic premise of the phenomenological model.

Several conclusions can be drawn from our findings. First of all, in view of Eqs. (16) and (18), the condition $|\alpha + \gamma K|^2 = |\beta|^2$ implies that an incident uniform unpolarized field emerges from the metallic double-slit structure into the far zone unpolarized. This is a kind of trivial case since nothing happens to the polarization state. Second, if instead $|\alpha + \gamma K|^2 \neq |\beta|^2$, our results show that a uniform linearly partially polarized input field can be rendered fully unpolarized, provided the coefficients (α , β , and γ) and K are chosen appropriately and the polarized part is either s polarized ($|\alpha + \gamma K| > |\beta|$) or p polarized ($|\beta| > |\alpha + \gamma K|$). This can always be arranged by suitably orienting the incident polarization. Third, it follows that elliptically (or circularly) partially polarized uniform fields cannot be made unpolarized in this way, since the polarized contribution has to be either a TE or a TM field and elliptical polarization states necessarily contain both.

Finally, we display in Fig. 7 explicit graphs of P^i , P , and the depolarization ratio P/P^i within the range where physically meaningful solutions of Eq. (16) are found. In Fig. 7(a) we show the results when the system parameters are the same as in Fig. 6. We observe that $P = 0$ only when $\phi = \pi/2$. The effects of surface plasmons are significant, as the differences between the solid and dashed lines demonstrate. We note that, according to Eq. (17), the allowed ϕ range is also widened by the SPPs. In Fig. 7(b) we show similar plots for a smaller slit separation $a = 50\lambda_{sp}$, in which case the plasmon effects are even more pronounced.

VI. CONCLUSION

We have considered the polarization state of the radiation emerging paraxially from a double-slit structure in a metal film under uniform, partially polarized illumination. Making use of rigorous numerical electromagnetic field computations (Fourier modal method), we have assessed the accuracy of a phenomenological model applicable to subwavelength slits

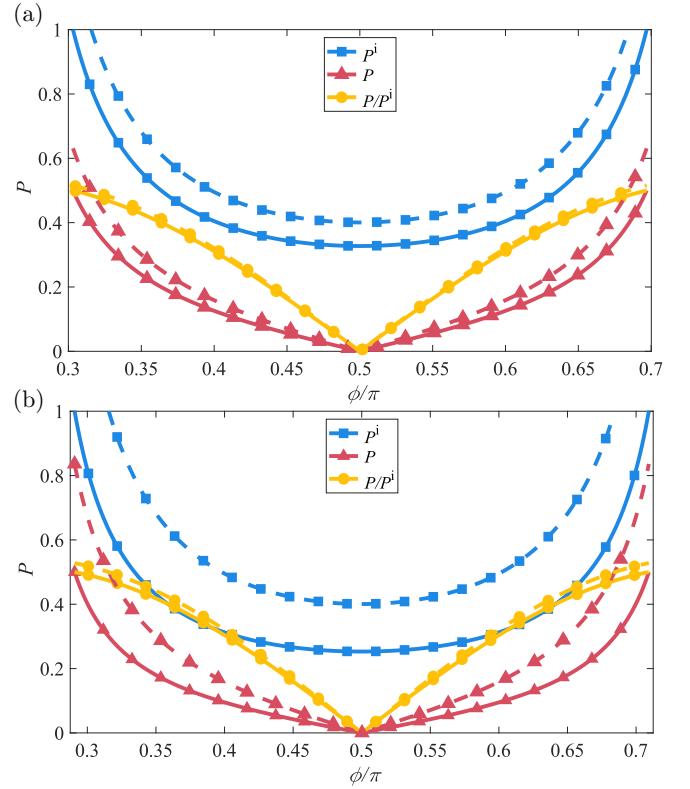


FIG. 7. Depolarization effects. The solid lines represent the cases (a) $a = 159\lambda_{sp}$ and (b) $a = 50\lambda_{sp}$. In both figures the dashed lines refer to the situation when the plasmon effects are ignored ($\gamma = 0$). All other parameters in both figures are as in Fig. 6.

of sufficient depth and incorporating the effects of surface plasmon propagation. We demonstrated that the simple intuitive model can accurately be used for any slit separation and plasmon propagation length as long as the former is large enough to ignore (multiple) SPP reflections between the slits. This required slit separation strongly depends on the metal and the incident-light wavelength and thus reflects the strength of the plasmon field. The plasmon-mediated interference allows one to control the far-zone polarization degree and state. In particular, we showed that a linearly, partially polarized incident field can, under suitable conditions, be rendered totally unpolarized.

ACKNOWLEDGMENTS

This research was funded by the Academy of Finland (Grants No. 310511 and No. 333938). It is part of the Academy of Finland's flagship program "Photonics Research and Innovation" (Program No. 320166). A.L. acknowledges funding from the Finnish Cultural Foundation; T.D.V. acknowledges support from NWO under Grant No. P19-13 and thanks the Joensuu University Foundation for support. G.W. was supported by the National Natural Science Foundation of China under Grant No. 12074310.

APPENDIX A: DERIVATION OF EQS. (2), (3), (8), and (12)

Using any suitable rigorous electromagnetic technique, we can determine the response of the structure separately in p and s (TM and TE) polarizations. Let us denote the transverse (x, y) components of the fields at $z = d$, arising from a unit-amplitude plane-wave illumination from $z < 0$, by $E_x(x, d)$ in p polarization and by $E_y(x, d)$ in s polarization. This can be done whether both slits are open or one of them is covered with a block preventing direct transmission.

The fields at $z = d$ can be propagated to an arbitrary plane $z > d$ using the angular spectrum technique

$$E_j(x, z) = \int_{-\infty}^{\infty} A_j(k_x) \exp[i(k_x x + k_z \Delta z)] dk_x, \quad (\text{A1})$$

where $\Delta z = z - d$,

$$A_j(k_x) = \frac{1}{2\pi} \int_{-\infty}^{\infty} E_j(x, d) \exp(-ik_x x) dx, \quad (\text{A2})$$

and

$$k_z = \begin{cases} \sqrt{k_0^2 - k_x^2} & \text{when } |k_x| < k_0 \\ i\sqrt{k_x^2 - k_0^2} & \text{when } |k_x| > k_0. \end{cases} \quad (\text{A3})$$

At distances $\Delta z \gg \lambda_0$ the contributions of the evanescent waves with imaginary values of k_z (giving rise to the plasmonic fields in p polarization) can be ignored. In such circumstances we may limit the spatial integration in Eq. (A2) to the close proximity of the slits.

At sufficiently large values of Δz the field $E_j(x, z)$ can be accurately described by an asymptotic expression

$$E_j(x, z) = \sqrt{2\pi k_0} \exp\left(-\frac{i\pi}{4}\right) s_z A_j(k_0 s_x) \frac{\exp(ik_0 r)}{\sqrt{r}}, \quad (\text{A4})$$

where $s_x = x/r$, $s_z = \Delta z/r$, and $r = \sqrt{x^2 + \Delta z^2}$. Although this formula is strictly valid in the limit $r \rightarrow \infty$, in practice it is a good approximation when $\Delta z \gg a$. In this paper we are interested only in the paraxial region. Here $r \approx \Delta z$, $s_z \approx 1$, and $s_x \approx x/\Delta z = \sin \theta \approx \theta$, where θ is the diffraction angle. Now Eq. (A4) reduces to

$$E_j(x, z) \approx \sqrt{2\pi k_0} \exp\left(-\frac{i\pi}{4}\right) A_j(k_0 \theta) \frac{\exp(ik_0 \Delta z)}{\sqrt{\Delta z}}. \quad (\text{A5})$$

This result holds for both p ($j = x$) and s ($j = y$) polarizations.

Allowing the incident plane-wave field to be partially polarized and representing it with Eq. (1), the action of the slit system (as regards the transverse electric field) can formally be described by a deterministic diagonal transmission (Jones) matrix $\mathbf{T}(x, d)$ with diagonal elements $E_x(x, d)$ and $E_y(x, d)$. The polarization matrix at the exit plane $z = d$ takes the form

$$\begin{aligned} \mathbf{J}(x, d) &= \mathbf{T}^*(x, d) \mathbf{J}^i(x, 0) \mathbf{T}^T(x, d) \\ &= \begin{bmatrix} J_{xx}(x, d) & J_{xy}(x, d) \\ J_{yx}(x, d) & J_{yy}(x, d) \end{bmatrix} \\ &= \begin{bmatrix} J_{pp}|E_x(x, d)|^2 & J_{ps}E_x^*(x, d)E_y(x, d) \\ J_{sp}E_y^*(x, d)E_x(x, d) & J_{ss}|E_y(x, d)|^2 \end{bmatrix}. \end{aligned} \quad (\text{A6})$$

The polarization properties in the paraxial region of the far zone are defined by a polarization matrix

$$\mathbf{J}(x, z) = \frac{2\pi k_0}{\Delta z} \mathbf{J}(\theta), \quad (\text{A7})$$

where

$$\begin{aligned} \mathbf{J}(\theta) &= \begin{bmatrix} J_{xx}(\theta) & J_{xy}(\theta) \\ J_{yx}(\theta) & J_{yy}(\theta) \end{bmatrix} \\ &= \begin{bmatrix} J_{pp}|A_x(k_0\theta)|^2 & J_{ps}A_x^*(k_0\theta)A_y(k_0\theta) \\ J_{sp}A_y^*(k_0\theta)A_x(k_0\theta) & J_{ss}|A_y(k_0\theta)|^2 \end{bmatrix} \end{aligned} \quad (\text{A8})$$

may be called the angular polarization matrix.

The phenomenological model employed in the main text follows if we formally take the slits to be line sources of appropriate strengths. When both slits are open, we may set

$$E_x(x, d) = \pi(\alpha + \gamma K) \left[\delta\left(x + \frac{a}{2}\right) + \delta\left(x - \frac{a}{2}\right) \right], \quad (\text{A9})$$

$$E_y(x, d) = \pi\beta \left[\delta\left(x + \frac{a}{2}\right) + \delta\left(x - \frac{a}{2}\right) \right]. \quad (\text{A10})$$

This gives

$$A_x(k_x) = (\alpha + \gamma K) \cos\left(\frac{ak_x}{2}\right), \quad (\text{A11})$$

$$A_y(k_x) = \beta \cos\left(\frac{ak_x}{2}\right), \quad (\text{A12})$$

leading to Eqs. (2) and (3). When only slit 1 is open (slit 2 is blocked) and the illumination is p polarized, we have

$$E_x(x, d) = 2\pi \left[\alpha \delta\left(x + \frac{a}{2}\right) + \gamma K \delta\left(x - \frac{a}{2}\right) \right], \quad (\text{A13})$$

$$A_x(k_x) = \alpha \exp\left(\frac{ik_x a}{2}\right) + \gamma K \exp\left(-\frac{ik_x a}{2}\right), \quad (\text{A14})$$

resulting in Eq. (9). When both slits are open but the illumination is strictly p polarized, we have Eqs. (A9) and (A11), leading to Eq. (12). We emphasize that because of the nature of the phenomenological model, only the relative values of the complex factors (α , β , and γ) are important in any given metal, slit, and illumination configuration.

APPENDIX B: FAR-ZONE POLARIZATION STATE

Let us represent the polarization matrix of the incident field as a sum of unpolarized and polarized parts [see [18], Eqs. (6.3–16) and (6.3–17)]

$$\mathbf{J}^i = \mathbf{J}_u^i + \mathbf{J}_p^i = A \begin{bmatrix} 1 & 0 \\ 0 & 1 \end{bmatrix} + \begin{bmatrix} B & D \\ D^* & C \end{bmatrix}, \quad (\text{B1})$$

with $BC - DD^* = 0$. Since we set $\text{tr} \mathbf{J}^i = 1$, we obtain $2A + B + C = 1$. If we also fix the degree of polarization

$$P^i = \frac{\text{tr} \mathbf{J}_p^i}{\text{tr} \mathbf{J}^i} = 1 - 2A, \quad (\text{B2})$$

we find that the elements of the decomposed matrix must satisfy the conditions

$$A = \frac{1 - P^i}{2}, \quad B + C = P^i, \quad |D|^2 = BC. \quad (\text{B3})$$

Taking the fully polarized part of the incident field to be linearly polarized, the conditions in Eq. (B3) lead to a representation

$$\mathbf{J}^i = \frac{1}{2}(1 - P^i) \begin{bmatrix} 1 & 0 \\ 0 & 1 \end{bmatrix} + P^i \begin{bmatrix} \cos^2 \phi & \sin \phi \cos \phi \\ \sin \phi \cos \phi & \sin^2 \phi \end{bmatrix}, \quad (\text{B4})$$

where ϕ is the polarization angle measured from the x direction. The elements of the far-field polarization matrix defined in Eq. (3) then read

$$\Phi_{xx} = [\frac{1}{2}(1 - P^i) + P^i \cos^2 \phi] |\alpha + \gamma K|^2, \quad (\text{B5})$$

$$\Phi_{xy} = P^i (\alpha + \gamma K)^* \beta \sin \phi \cos \phi, \quad (\text{B6})$$

$$\Phi_{yx} = P^i (\alpha + \gamma K) \beta^* \sin \phi \cos \phi, \quad (\text{B7})$$

$$\Phi_{yy} = [\frac{1}{2}(1 - P^i) + P^i \sin^2 \phi] |\beta|^2. \quad (\text{B8})$$

The Stokes parameters associated with the matrix Φ take the explicit forms

$$S_0 = \frac{1}{2} [|\alpha + \gamma K|^2 + |\beta|^2 + P^i (|\alpha + \gamma K|^2 - |\beta|^2) \cos(2\phi)], \quad (\text{B9})$$

$$S_1 = \frac{1}{2} [|\alpha + \gamma K|^2 - |\beta|^2 + P^i (|\alpha + \gamma K|^2 + |\beta|^2) \cos(2\phi)], \quad (\text{B10})$$

$$S_2 = P^i \text{Re}[(\alpha + \gamma K)^* \beta] \sin(2\phi), \quad (\text{B11})$$

$$S_3 = P^i \text{Im}[(\alpha + \gamma K)^* \beta] \sin(2\phi), \quad (\text{B12})$$

where, as before, Re and Im denote the real and imaginary parts, respectively.

-
- [1] T. W. Ebbesen, H. J. Lezec, H. F. Ghaemi, T. Thio, and P. A. Wolff, Extraordinary optical transmission through subwavelength hole arrays, *Nature (London)* **391**, 667 (1998).
 - [2] J. A. Porto, F. J. García-Vidal, and J. B. Pendry, Transmission Resonances on Metallic Gratings with Very Narrow Slits, *Phys. Rev. Lett.* **83**, 2845 (1999).
 - [3] H. F. Schouten, T. D. Visser, D. Lenstra, and H. Blok, Light transmission through a subwavelength slit: Waveguiding and optical vortices, *Phys. Rev. E* **67**, 036608 (2003).
 - [4] J. Lindberg, K. Lindfors, T. Setälä, M. Kaivola, and A. T. Friberg, Spectral analysis of resonant transmission of light through a single subwavelength slit, *Opt. Express* **12**, 623 (2004).
 - [5] M. L. Brongersma and P. G. Kik, *Surface Plasmon Nanophotonics* (Springer, Berlin, 2007).
 - [6] W. L. Barnes, A. Dereux, and T. W. Ebbesen, Surface plasmon subwavelength optics, *Nature (London)* **424**, 824 (2003).
 - [7] J. Homola, S. S. Yee, and G. Gauglitz, Surface plasmon resonance sensors, *Sensor. Actuat. B* **54**, 3 (1999).
 - [8] D. Wang, W. Wang, M. P. Knudson, G. C. Schatz, and T. W. Odom, Structural engineering in plasmon nanolasers, *Chem. Rev.* **118**, 2865 (2018).
 - [9] A. Safaei, S. Modak, A. Vázquez-Guardado, D. Franklin, and D. Chandra, Cavity-induced hybrid plasmon excitation for perfect infrared absorption, *Opt. Lett.* **43**, 6001 (2018).
 - [10] Y. Chen, A. Norrman, S. A. Ponomarenko, and A. T. Friberg, in *Progress in Optics*, edited by T. D. Visser (Elsevier, Amsterdam, 2020), Vol. 65, pp. 105–172.
 - [11] H. F. Schouten, N. Kuzmin, G. Dubois, T. D. Visser, G. Gbur, P. F. A. Alkemade, H. Blok, G. W. 't Hooft, D. Lenstra, and E. R. Eliel, Plasmon-Assisted Two-Slit Transmission: Young's Experiment Revisited, *Phys. Rev. Lett.* **94**, 053901 (2005).
 - [12] C. H. Gan, G. Gbur, and T. D. Visser, Surface Plasmons Modulate the Spatial Coherence of Light in Young's Interference Experiment, *Phys. Rev. Lett.* **98**, 043908 (2007).
 - [13] S. Divitt, M. Frimmer, T. D. Visser, and L. Novotny, Modulation of optical spatial coherence by surface plasmon polaritons, *Opt. Lett.* **41**, 3094 (2016).
 - [14] H. Kim, J. Park, and B. Lee, *Fourier Modal Method and its Applications in Computational Nanophotonics* (CRC Press, Boca Raton, 2017).
 - [15] H. Raether, *Surface Plasmons on Smooth and Rough Surfaces and on Gratings* (Springer, Berlin, 1988).
 - [16] C. Brosseau, *Fundamentals of Polarized Light: A Statistical Optics Approach* (Wiley, New York, 1988).
 - [17] D. Morrill, D. Li, and D. Pacifici, Measuring subwavelength spatial coherence with plasmonic interferometry, *Nat. Photon.* **10**, 681 (2016).
 - [18] L. Mandel and E. Wolf, *Optical Coherence and Quantum Optics* (Cambridge University Press, Cambridge, 1995).